

The WISSH quasars project

VI. Fraction and properties of BAL quasars in the hyper-luminosity regime

G. Bruni¹, E. Piconcelli², T. Misawa³, L. Zappacosta², F. G. Saturni^{2,4}, G. Vietri^{5,6}, C. Vignali^{7,8}, A. Bongiorno², F. Duras^{9,2}, C. Feruglio^{10,2}, F. Tombesi^{11,12,13,2}, and F. Fiore¹⁰

¹ INAF - Istituto di Astrofisica e Planetologia Spaziali, via Fosso del Cavaliere 100, 00133 Roma, Italy
e-mail: gabriele.bruni@inaf.it

² INAF - Osservatorio Astronomico di Roma, via Frascati 33, 00040 Monte Porzio Catone, Roma, Italy

³ School of General Education, Shinshu University 3-1-1 Asahi, Matsumoto, 390-8621, Japan

⁴ ASI - Space Science Data Center, via del Politecnico snc, 00133 Roma, Italy

⁵ Excellence Cluster Universe, Technische Universität München, Boltzmannstr. 2, 85748 Garching, Germany

⁶ European Southern Observatory, Karl-Schwarzschild-Str. 2, 85748 Garching bei München, Germany

⁷ DiFA - Dipartimento di Fisica e Astronomia, Università degli Studi di Bologna, Via Gobetti 93/2, 40129 Bologna, Italy

⁸ INAF - Osservatorio di Astrofisica e Scienza dello Spazio di Bologna, Via Piero Gobetti 93/3, 40129 Bologna, Italy

⁹ Dipartimento di Matematica e Fisica, Università degli Studi Roma Tre, Via della Vasca Navale 84, 00146 Roma, Italy

¹⁰ INAF - Osservatorio Astronomico di Trieste, Via G.B. Tiepolo 11, 34143 Trieste, Italy

¹¹ Dipartimento di Fisica, Università degli Studi di Roma "Tor Vergata", Via della Ricerca Scientifica 1, 00133 Roma, Italy

¹² Department of Astronomy, University of Maryland, College Park, MD 20742 USA

¹³ NASA/Goddard Space Flight Center, Code 662, Greenbelt, MD 20771 USA

ABSTRACT

Context. The WISSH quasars project aims at studying the nuclear and host galaxy properties of the most luminous quasars ($L_{bol} > 10^{47}$ erg/s, $1.8 < z < 4.6$), with special emphasis on the occurrence and physical parameters of winds at different scales.

Aims. Nuclear winds are manifested as UV broad ($\geq 2,000$ km/s) absorption lines (BAL) in $\sim 15\%$ of quasars. We aim at studying the incidence and properties of such winds in the WISSH sample, to investigate possible differences with respect to lower luminosity AGN regimes.

Methods. We collected optical spectra from the SDSS data release 12, and identified those showing absorption troughs in the region between Si IV and C IV emission lines. We used three different indices for BAL absorption: the classic Balnicity Index (BI), the Absorption Index (AI), and the intermediate AI_{1000} .

Results. We find a higher observed fraction of C IV BAL quasars in the WISSH sample (24%) with respect to previous catalogues (10-15%). These WISSH BAL quasars are also characterized by a larger average BI ($\sim 4,000$ km/s) and maximum velocity ($\sim 17,000$ km/s). Moreover, for two objects we discovered BAL features bluewards of the Si IV peak, which can be associated to C IV absorption with velocity of 0.15c. Finally, we updated previous studies on the dependence of maximum outflow velocity upon bolometric luminosity, showing that BAL winds have intermediate properties compared to molecular/ionized winds and ultra fast outflows (UFOs). Finally, the radio properties of the WISSH BAL quasars as a whole are in line with those of samples at lower luminosities from previous studies.

Conclusions. Our results suggest that the higher L_{bol} of the WISSH quasars likely favours the acceleration of BAL outflows and that their most likely driving mechanism is radiation pressure. Furthermore we estimate that the kinetic power associated to these winds in hyperluminous quasars is sufficient, for the highest column density and fastest winds, to provide efficient feedback onto the host galaxy.

Key words. galaxies:active; galaxies: nuclei - quasars: absorption lines; quasars:general; quasars: supermassive black holes - ISM: jets and outflow

1. Introduction

In the last two decades, there has been growing recognition of the potential importance of quasar (QSOs) winds for the growth of super-massive black holes (SMBH, Silk & Rees 1998), enrichment of the intergalactic medium (Li et al. 2007), galaxy formation (Haiman & Bryan 2006), evolution of the host galaxy (Di Matteo et al. 2005), and the luminosity function of quasars (Wyithe & Loeb 2003). The Active Galactic Nucleus (AGN) power is fundamental in the overall winds dynamics, thus bolometric luminosity (L_{bol}) and Eddington ratio are key quantities to understand the feedback mechanism on the host galaxy. Interac-

tion of radiation, jets, and winds with the interstellar medium of the host is often invoked as responsible of star-formation quenching and growth regulation, and commonly explained with two main scenarios: the radio-mode, and the quasar-mode one (see Fabian 2012 for a review). In the former, the collimated radio jet is responsible for removing - through fast shocks - the ambient gas, while in the latter the main cause is identified in fast, nuclear winds. Recently, both scenarios have proven to be valid: radio-mode feedback has been studied by Tadhunter et al. (2014), who presented evidences of a molecular outflow accelerated by the jet in a Seyfert galaxy, while Tombesi et al. (2015) and Feruglio et al. (2015) pointed out that highly-ionized, mas-

sive SMBH winds with velocity of $0.1-0.2c$ are likely the drivers of kpc-scale molecular winds with large outflow rates, i.e. $\geq 500 M_{\odot}/\text{yr}$ (see Bischetti et al. 2019 for a more complete picture).

Nuclear winds from the accretion disk can be observed in the UV domain as broad absorption lines (BALs) blue-wards of prominent emission lines (e.g. C IV, Si IV) in 10-20% of optically-selected quasars. They trace wind velocities from a few thousands km/s up to $\sim 0.3c$ (e.g. Hewett & Foltz 2003; Hamann et al. 2018). Depending on the involved species, BALs are divided into high-ionization (HiBALs) and low-ionization (LoBALs): while high-ionization species (C IV, Si IV, N V) always produce the most prominent absorption features in these objects, about 15% shows also troughs blue-wards of lower-ionization species like Mg II and Al III. Additionally, are termed FeLoBALs the LoBALs showing also Fe II and Fe III absorption features. The number of known BAL QSOs has greatly increased in recent years, thanks to the several data releases of the Sloan Digital Sky Survey (SDSS, York et al. 2000), reaching more than 20,000 objects in the recent releases of the SDSS quasar catalogue (Pâris et al. 2017, 2018). This allowed detailed studies of statistically complete samples, helping in characterizing the BAL phenomenology (see Sec. 3 for a complete discussion). Notwithstanding, a comprehensive scheme for the launching and geometry of BAL winds is still missing, although some attempts of constructing reasonable scenarios exist (Murray & Chiang 1995; Proga 2000; Elvis 2000; Risaliti & Elvis 2010). Despite theoretical models suggest that these winds should be launched by the accretion disk, at a radius smaller than 1 pc (e.g. Proga 2000; Elvis 2000), to date observational results suggest that the distance at which the absorption occurs ranges from several tens to thousands parsecs, with larger radii for luminous quasars (see e.g. Arav et al. 2013; Hemler et al. 2019 and references therein). Lately, Arav et al. (2018) found evidence that 50% of BAL winds extend at least 100 pc from the nucleus, in a sample of ~ 20 high-luminosity quasars. This highlights that these ionized outflows could indeed represent an important source of feedback to the host galaxy, although this is not in line with previous claims that BAL winds are located at scales of the AGN accretion disk.

Similarly, Ultra Fast Outflows (UFOs) are of nuclear origin as well but detected as absorption troughs in the X-ray domain, tracing higher-ionization species at mildly relativistic velocities $> 0.1c$ (Tombesi et al. 2010, 2011). The origin of both BAL and UFO winds should reside in the accretion disk, and be driven by radiation pressure or magnetohydrodynamic processes (Laor & Brandt 2002; Tombesi et al. 2013; Kraemer et al. 2018). Radio emission from the jet was used by different authors as indicator of the outflow orientation in samples of radio-loud BAL QSOs, not finding a clear hint of a preferred one (Montenegro-Montes et al. 2008; DiPompeo et al. 2011; Bruni et al. 2012). VLBI observations showed a variety of morphologies (Bruni et al. 2013) also not pointing towards a particular angle, suggesting that the presence of BAL outflows and the consequent fraction of these objects among quasars should be due to inner physical properties of the AGN, and not to a mere orientation effect. Indeed, indications of an anticorrelation with radio loudness has been found (Becker et al. 2000; Gregg et al. 2006; Shankar et al. 2008), while Hewett & Foltz (2003) suggested that optically-bright BAL QSOs are half as likely as non-BAL QSOs to have $S_{1.4\text{GHz}} > 1 \text{ mJy}$.

AGN winds at different scales are expected to increase their momentum and kinetic power with AGN bolometric luminosity (Menci et al. 2008; Zubovas & King 2012; Costa et al. 2014). There is mounting evidence that this prediction is correct based on observations at different wavelength of outflows involving

different gas phases and distances from the SMBH (e.g., Cicone et al. 2014; Matzeu et al. 2017; Fiore et al. 2017). We have therefore undertaken a multi-band (from millimeter to X-rays) follow-up of a sample of 86 WISE/SDSS selected hyper-luminous (WISSH) quasars in the redshift range $z \approx 2 - 4$, i.e. the so-called ‘cosmic noon’ at the peak of star formation activity and QSO number density. The major goal is to provide a detailed investigation of nuclear and host galaxy properties and the census of AGN-driven winds in sources at the brightest end of the AGN luminosity function. WISSH QSOs exhibit very high bolometric luminosity ($L_{\text{bol}} \gtrsim 10^{47} \text{ erg/s}$) powered by highly-accreting, ultra-massive ($> 10^9 M_{\odot}$) SMBHs (see Bischetti et al. 2017; Duras et al. 2017; Martocchia et al. 2017; Vietri et al. 2018). These hyper-luminous AGN are thus expected to launch the most powerful outflows. By analyzing rest-frame UV and optical spectra of WISSH QSOs, Bischetti et al. (2017); Vietri et al. (2018) indeed reported on the discovery of ionized outflows both on kpc- and pc-scale, with extreme properties in terms of velocity and kinetic energy.

In this paper, we present a study of the fraction and properties of the BAL QSOs in the WISSH sample, discussing their dependence on the extreme bolometric luminosities of these objects. We adopt the latest cosmological parameters from the *Planck* mission (Planck Collaboration et al. 2018), i.e. assuming the base- Λ CDM cosmology: $H_0 = 67.4 \text{ km/s/Mpc}$, $\Omega_m = 0.315$, and $\Omega_{\Lambda} = 0.685$.

2. BAL identification from SDSS DR12 spectra

We performed a detailed search of BAL QSOs in the WISSH sample of 86 hyper-luminous QSOs, making use of SDSS optical spectra. At the mean redshift of the sample ($z \sim 3.2$) the SDSS observer’s frame wavelength range (3500-9000 Å) corresponds to 830-2140 Å in the rest-frame, allowing to explore the whole region between Ly α and Al III emission lines. Our aim was to test whether the BAL fraction, and thus the presence of nuclear winds, is different at high-luminosity regime, comparing with previous estimates from the literature at lower luminosity ($L_{\text{bol}} < 10^{47} \text{ erg/s}$). In the following, the method and details for BAL QSOs selection are given.

We collected optical spectra of all the 86 WISSH objects from the 12th data release of the SDSS (Alam et al. 2015). As a first selection step, we visually inspected them to find footprint of absorption features blue-wards of the C IV emission peak. This led us to 42 candidate BAL QSOs ($\sim 48\%$ of the sample). Then, we fitted their spectra with the `continuum` tool in IRAF¹, using `spline3` as polynomial function, and flagging all the points part of the C IV absorption feature. With the obtained residuals, we characterized in velocity space the broad absorption feature making use of three well-known indices from the literature: 1) the Absorption Index (AI), as defined in Hall et al. (2002),

$$\text{AI} = \int_0^{25000} \left(1 - \frac{f(v)}{0.9}\right) \cdot C dv, \quad (1)$$

where the parameter C is unity over contiguous troughs of at least 450 km/s; 2) the modified Absorption Index (AI_{1000} , Bruni et al. 2012), defined as in Hall et al. (2002), but where the parameter C is unity over contiguous troughs of at least 1,000 km/s (as in Trump et al. 2006); 3) the Balnicity Index (BI), as defined by Weymann et al. (1991),

$$\text{BI} = \int_{3000}^{25000} \left(1 - \frac{f(v)}{0.9}\right) \cdot C dv, \quad (2)$$

¹ <http://iraf.noao.edu/>

Table 1: The 40 BAL QSOs from the WISSH sample: the first 38 objects are identified through absorption features between the Si iv and C iv emission lines, while the last two ones from features blue-wards of Si iv. Absorption indices estimates are given in columns 4-6. In the last column, the BAL type is reported: objects with a C iv BI>0 are in bold face, while "BAL" means that the spectrum coverage does not allow a proper HiBAL/LoBAL classification. Starred redshifts are from Vietri et al. (2018).

ID	SDSS ID	z	AI	AI ₁₀₀₀	BI	v_{min}	v_{max}	Type
(1)	(2)	(3)	[km/s]	[km/s]	[km/s]	[km/s]	[km/s]	(9)
0045+14	SDSS004527.68+143816.1	1.992	7762	7718	7016	1300	16000	LoBAL
0216-09	SDSS021646.94-092107.2	3.691	2335	1940	1170	8770	18800	HiBAL
0414+06	SDSS041420.90+060914.2	2.614*	10806	10285	7415	1140	13750	HiBAL
0747+27	SDSS074711.14+273903.3	4.110	209	12	0	2940	12680	BAL
0928+53	SDSS092819.29+534024.1	4.390	9217	8327	8327	3430	19050	BAL
0959+13	SDSS095937.11+131215.4	4.061	29	0	0	13800	15700	BAL
1013+56	SDSS101336.37+561536.3	3.633	127	0	0	3460	11650	HiBAL
1025+24	SDSS102541.78+245424.2	2.382	3059	2866	2356	7260	13750	LoBAL
1048+44	SDSS104846.63+440710.8	4.347	11125	10720	9044	2060	17840	BAL
1051+31	SDSS105122.46+310749.3	4.243	203	14	0	9920	11800	BAL
1103+10	SDSS110352.74+100403.1	3.590	357	38	0	1530	6160	HiBAL
1110+19	SDSS111017.13+193012.5	2.498	2680	2532	0	590	4900	HiBAL
1110+48	SDSS111038.63+483115.6	2.957	145	0	0	14360	15440	HiBAL
1122+16	SDSS112258.77+164540.3	3.024	8061	7861	7312	6610	17670	LoBAL
1130+07	SDSS113017.37+073212.9	2.654	25	0	0	10710	12140	HiBAL
1157+27	SDSS115747.99+272459.6	2.217*	5641	4948	4021	2000	17200	HiBAL
1204+33	SDSS120447.15+330938.7	3.596	5282	5117	3531	1620	10590	LoBAL
1210+17	SDSS121027.62+174108.9	3.604*	5903	5595	5116	5840	14750	HiBAL
1215-00	SDSS121549.81-003432.1	2.707	1679	1289	399	5800	20640	HiBAL
1237+06	SDSS123714.60+064759.5	2.781	872	187	0	4200	19810	HiBAL
1245+01	SDSS124551.44+010505.0	2.798	3707	3530	1939	1300	12300	HiBAL
1250+20	SDSS125050.88+204658.7	3.570	890	824	0	350	3820	HiBAL
1305+05	SDSS130502.28+052151.1	4.071	246	42	0	19500	22550	HiBAL
1326-00	SDSS132654.96-000530.1	3.303*	2275	1960	0	0	3850	HiBAL
1328+58	SDSS132827.06+581836.8	3.133	322	131	0	3500	5400	HiBAL
1422+44	SDSS142243.02+441721.2	3.648*	310	0	0	15410	22780	HiBAL
1447+10	SDSS144709.24+103824.5	3.699	6179	4484	65	370	23520	HiBAL
1451+14	SDSS145125.31+144136.0	3.102	4848	4340	3586	6000	13400	HiBAL
1506+52	SDSS150654.55+522004.7	4.068	5147	4938	4396	12970	23130	HiBAL
1513+08	SDSS151352.52+085555.7	2.897	1293	820	0	200	4800	HiBAL
1544+41	SDSS154446.34+412035.7	3.548	4808	4663	4270	9580	23500	HiBAL
1549+12	SDSS154938.72+124509.1	2.365*	4918	4425	1735	0	6470	HiBAL
1555+10	SDSS155514.85+100351.3	3.512	6992	6490	5576	7090	16000	LoBAL
1633+36	SDSS163300.13+362904.8	3.576	377	241	90	18700	24800	HiBAL
1639+28	SDSS163909.10+282447.1	3.801	366	259	0	22300	28460	HiBAL
1650+25	SDSS165053.78+250755.4	3.338	3675	3516	2913	5000	13100	HiBAL
2123-00	SDSS212329.46-005052.9	2.282*	107	0	0	13500	24600	HiBAL
2238-08	SDSS223808.07-080842.1	3.122	4300	3889	2228	1500	19000	HiBAL
0947+14	SDSS094734.19+142116.9	3.040	795	685	548	41250	46040	HiBAL
1538+08	SDSS153830.55+085517.0	3.567*	439	318	130	38300	47000	HiBAL

where the parameter C is unity over contiguous troughs of at least 2,000 km/s. To perform this calculation, the spectral region between the peaks of the C iv and Si iv emission lines was integrated up to 25,000 km/s from the former, starting from a minimum detachment of 0 km/s for AI and AI₁₀₀₀, while 3,000 km/s for BI. The three indices are increasingly conservative, from AI to BI, AI₁₀₀₀ being the one that allows to study a variety of absorption features, but still filtering the most ambiguous ones. Although they can be considered as velocity-weighted equivalent widths, they do not directly measure any outflow physical quantity, but instead can be used to quantify the strength and width of the absorption for BAL QSOs identification purposes. Two among the objects presented here (0414+06 and 1210+17) are newly found BAL QSOs, since not present in previous BAL cat-

alogues (Trump et al. 2006; Gibson et al. 2009; Allen et al. 2011) or flagged as BAL in the latest editions of the SDSS QSOs catalogue (Pâris et al. 2014, 2017 - the latter extracted from SDSS DR12 as for our sample). Both objects show issues in the spectrum, that most probably misled the algorithm used for the compilation of previous catalogues: 0414+06 presents a spike in correspondence of the C iv peak, while 1210+17 has a spike at the right edge of the spectrum, and a very faint Ly- α line, that does not allow to easily identify the Si iv and C iv emission lines. For both objects a wrong redshift is given in SDSS, so we provide the corrected estimate in Tab. 1. In total, we found in WISSH 38 objects with an AI>0 (44±7%), 32 with AI₁₀₀₀ >0 (37±6%), and 21 with BI>0 (24±5%), whose uncertainties are calculated with

Poissonian statistic. Spectra for all the 38 BAL QSOs are given in appendix.

In addition to the classic selection based on C iv, we also looked for additional absorption from other species known to show BAL features, namely Si iv and Al iii (Mg ii was not covered by the spectra), with the aim to perform a HiBAL/LoBAL classification. In order to quantify the absorption for these two species we used a modified version of the previous indices, shifting the integration range blue-wards of the Si iv and Al iii emission lines, respectively, and adopting the same maximum velocity of 25,000 km/s. Two objects show strong BAL features blue-wards of the Si iv emission line, while only narrow absorption in the range between Si iv and C iv: we discuss these two particular cases in section 3.3. For 5 objects the redshift did not allow us to have the Al iii emission line region in the SDSS wavelength range, so the HiBAL/LoBAL classification was not possible. For all of the other sources the classification is given in Tab. 1.

3. BAL fraction and strength at the extreme luminosity regime

3.1. The BAL fraction in WISSH

The observed fraction of BAL QSOs (\mathcal{F}_{obs}) in the total AGN population has been explored by several authors since the early 2000s. The main works trying to compile BAL QSOs catalogues and study their characteristics are the following: 1) Hewett & Foltz (2003), presenting a sample of 67 BAL QSOs from the large bright quasar survey (Hewett et al. 1995, pre-SDSS era), resulting in a $\mathcal{F}_{obs}=15\pm3\%$; 2) Reichard et al. (2003), producing the first catalogue from SDSS early data release, including more than 200 objects, giving $\mathcal{F}_{obs}=14.0\pm1.0$; 3) Trump et al. (2006), from SDSS DR3, $\mathcal{F}_{obs}\sim10.4\%$; 4) Knigge et al. (2008), from SDSS DR3, $\mathcal{F}_{obs}=13.5$; 5) Gibson et al. (2009) (G09 hereafter), from SDSS DR5 as well, $\mathcal{F}_{obs}=13.3\pm0.6\%$; 6) Allen et al. (2011), the latest one, from SDSS DR6, finding a dependence from redshift and a $\mathcal{F}_{obs} = 8.0 \pm 0.1\%$. The common criterion adopted in the mentioned works to estimate \mathcal{F}_{obs} is the C iv BI. Considering the same definition of BAL QSO, we find in WISSH an observed fraction $\mathcal{F}_{obs}^W=24\pm5\%$ having a C iv BI>0: this is almost twice the average fraction found in previous works, and 9% more than the largest one among them. This points towards a intrinsic difference among WISSH BAL QSOs and previous samples, possibly linked to the hyper-luminosity regime. Dai et al. (2008) investigated \mathcal{F}_{obs} among 2MASS-selected QSOs: they claimed a value of $\sim 40\%$, finding that BAL QSOs are redder than non-BAL QSOs, and suggesting that a negative selection bias prevents from correctly estimating \mathcal{F}_{obs} in the optical band. Nevertheless, they found that a more restrictive classification based in BI leads to a $\mathcal{F}_{obs} \sim 20 - 23\%$ (see their Fig. 6), more similar to the fractions found from optical band studies. This value is directly comparable, and in agreement, with the fraction we are finding for our sources. We also note that their 2MASS-selection (i.e. $K_s < 15.1$ mag) for $z > 1.7$ sources implies a selection of the most luminous QSOs with $M_{K_s} < -30$ mag in the optical rest-frame band². Indeed as stated by Dai et al. (2008), only $\sim 5\%$ of SDSS QSOs are detected in 2MASS, as the latter is significantly shallower than the former. This suggests that the luminosity mainly drives the increase in the BAL fraction.

We could also estimate the fraction of LoBALs among BAL QSOs in WISSH. Indeed, for 19 objects among the 21 ones with

² Notice that the centroid of the K_s filter is centered in the rest-frame range 4000 – 8000Å for their sources at $z = 1.7 - 4.38$.

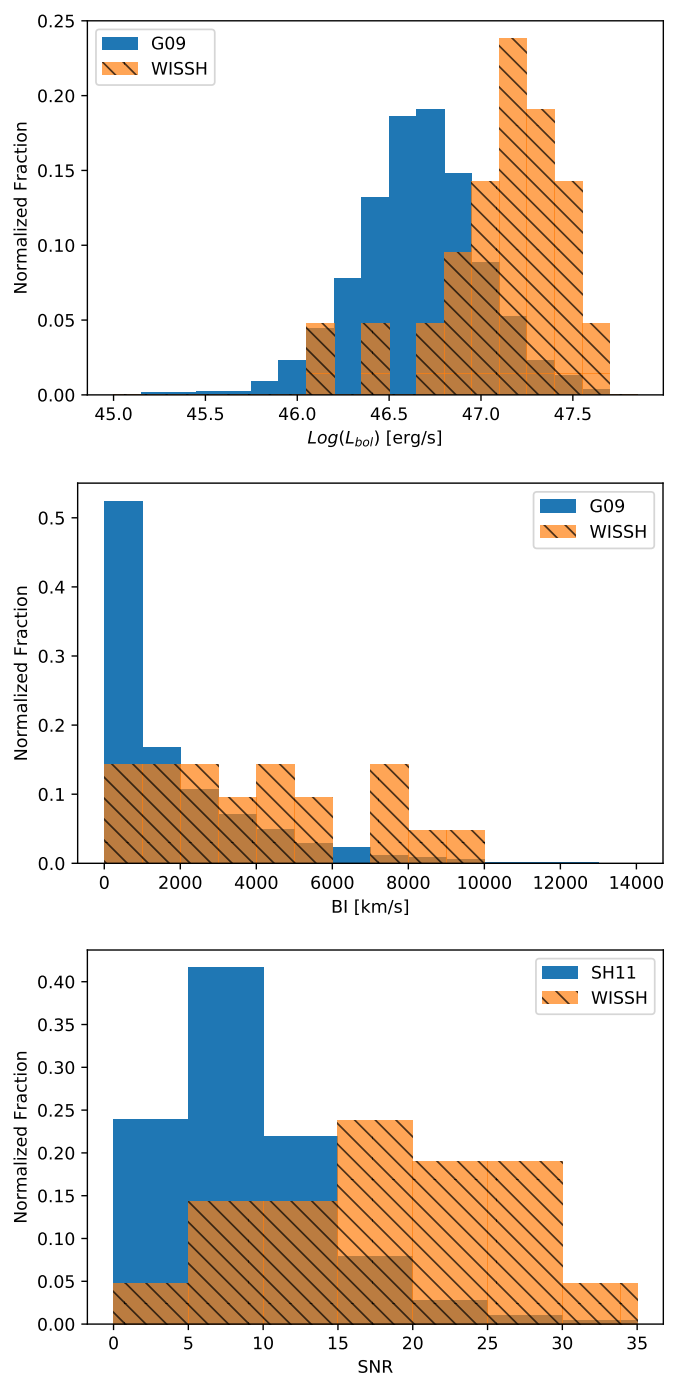


Fig. 1: Top panel: bolometric luminosity normalized distributions for WISSH and G09 objects with C iv BI>0; middle panel: C iv BI distribution for the WISSH sample and the BAL QSOs catalogue from Gibson et al. (2009); bottom panel: normalized distributions for the 1500-1600 Å SNR values extracted from SDSS DR7, for C iv BI>0 BAL QSOs in WISSH and in the Shen et al. (2011) QSO catalogue (SH11).

BI>0 the spectrum covers the Al iii region, allowing the LoBAL classification: for 5 over 19 we obtained a Al iii BI>0, giving a LoBAL fraction of $\sim 26_{-11}^{+18}\%$ (following Poissonian statistics for small numbers, see Gehrels 1986). Generally, LoBALs can be easily missed in large surveys, due to reddening and complex spectral features. The fraction found in WISSH is compatible within the errors with the one reported in the literature for SDSS

objects ($\sim 15\%$; e.g., Reichard et al. 2003; Sprayberry & Foltz 1992). Nevertheless, considering all C IV BI >0 from G09, and applying the same criterium as above for LoBAL identification (i.e. C IV BI >0 and Al III BI >0), we find a much lower LoBAL fraction of $6.5\pm 0.4\%$: this could indicate that at the WISSH hyper-luminosity regime not only highly-ionized gas outflows are more common, but also the lower-ionized component - possibly launched from larger accretion disk radii - can more easily reach the relativistic velocities needed to produce BAL troughs.

In the rest of the paper we will consider the G09 catalogue as the comparison sample, since it provides a more complete collection of wind parameters to be compared with our sample. In addition to that, we consider some quantities estimated in the Shen et al. (2011) QSOs catalogue, based on SDSS DR7, that adopt the BAL classification of G09. Considering all objects from G09 with a C IV BI >0 , we have a comparison sample of 4,242 objects with redshift in the range $1.5 < z < 5.0$. In order to study the BAL winds dependence on L_{bol} , and compare the G09 sample with the hyper-luminous objects from WISSH, we cross-correlated the C IV BI >0 sample above with the Shen et al. (2011) QSOs catalogue (1 arcsec match in position) as this work provides the L_{bol} estimates needed for our analysis. This reduces the number of comparison BAL QSO objects to 3874. Fig. 1 (top panel) shows the L_{bol} distributions for the C IV BI >0 objects from G09 and WISSH, and highlights the extreme values of L_{bol} covered by the WISSH QSOs with respect to the previous samples.

3.2. BI distribution and BAL strength

As a further comparison with the G09 BAL QSOs population, we investigated the BI distributions for all objects having a C IV BI >0 from G09 and from the WISSH sample: an excess of high BI values is found (see Fig. 1). A Kolmogorov-Smirnov (KS) test gives a $p < 0.05$ for the two distributions to be drawn from the same one.

G09 found a dependence of the BAL fraction from the spectra Signal-to-Noise Ratio (SNR), with a higher SNR in the C IV region favoring the identification of BAL troughs, and thus enhancing the fraction of BAL QSOs for a given sample. The WISSH sample is composed by high-luminosity objects (see Fig. 1), thus a higher SNR is expected. To verify how much this effect could influence the fraction we measured in WISSH, we extracted the SNR of the 1500-1600 Å rest-frame, non-absorbed, region from the Shen et al. (2011) quasar catalogue for the objects with a BI >0 in WISSH, and for all the objects flagged as BAL (as noted before, the Shen et al. 2011 BAL classification is taken from G09, and therefore it allows for a proper comparison). In Fig. 1, we compare the SNR distribution for WISSH BI >0 objects with the one for all the BI >0 objects from Shen et al. (2011). The mean SNR value increases in the two sets, from a value of 9 per pixel for the Shen et al. (2011) one, to 18 for WISSH. Following G09, an SNR increase from 9 to 18 should imply a variation of about 2% more BAL QSOs. This is clearly a too low contribution to justify the higher BAL QSOs fraction we see in the WISSH sample with respect to the literature.

3.3. Detection of Ultra-fast BAL Outflows (UBOs)

In addition to the 38 C IV BAL QSOs presented in the previous section, we could identify two more objects (0947+14 and 1538+08) showing BAL signatures blue-wards of the Si IV emission line, but only very narrow absorption troughs between the

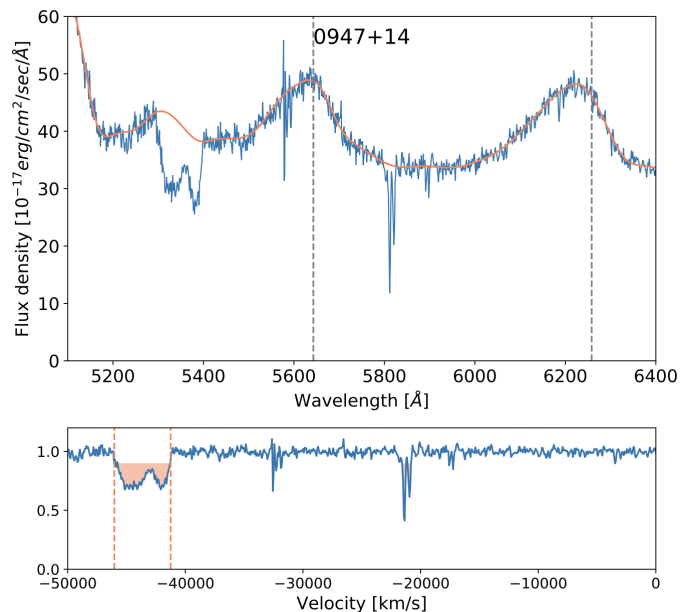


Fig. 2: Zoom on the C IV and Si IV regions for 0947+14 (SDSS DR12 spectrum), one of the two objects showing ultra-fast ($>0.1c$) BAL signatures associated to C IV absorption, blue-wards of the Si IV emission line. Top panel: spectrum (blue line) and fit performed in IRAF; dashed lines indicate the position of the Si IV and C IV peaks as calculated from redshift. Bottom panel: residuals between the C IV peak and $-50,000$ km/s, with absorption below 90% of the continuum highlighted in orange; dashed lines indicate the minimum and maximum velocity estimated for the BAL outflow.

C IV and Si IV lines (see Fig. 2). The optical depth ratio of the two species varies as a function of the ionisation parameter U , and for values typically found in BAL QSOs ($\text{Log}(U) > -2$) C IV dominates the Si IV depth by a factor of ~ 2 (Dunn et al. 2012). The absence of strong absorption between the Si IV and C IV lines can thus suggest that the BAL on the left side of Si IV is indeed due to C IV. This leads to a maximum velocity for the outflows in 0947+14 and 1538+08 of $0.15c$ and $0.16c$, respectively. These ultra-fast BAL outflows (UBOs) - that we could conveniently define as the ones having a maximum velocity larger than $0.1c$, allowing them to show C IV absorption blue-wards of the Si IV emission peak - are among the most extreme ones detected to date. Although less common than slower BAL outflows, there is a growing census of UBOs in the literature (Rodríguez-Hidalgo et al. 2011; Hamann et al. 2013; Rogerson et al. 2016), presenting in some cases C IV absorption troughs bluewards of the Ly α peak, implying a velocity of $\sim 0.3c$ (Hamann et al. 2018). A detailed analysis of multi-epoch UBOs properties in the WISSH sample will be presented in a forthcoming paper (Piconcelli et al. in prep.).

We explored the relative abundance of such relativistic BAL features in G09, by identifying all objects having a Si IV BI >0 and a C IV BI $=0$ in analogy to the two ones found in WISSH. In total, $2.9\pm 0.3\%$ of objects in G09 show such characteristics (127 over the 4369 ones having Si IV or C IV BI >0), while the fraction we obtain for WISSH is $9_{-6}^{+11}\%$ (2 over 23 objects, i.e. the 21 C IV BI >0 BAL QSOs plus the 2 UBOs themselves). This hints to a possible larger fraction of UBOs in high-luminosity QSOs such as WISSH. However, the very limited statistics hampers any firm

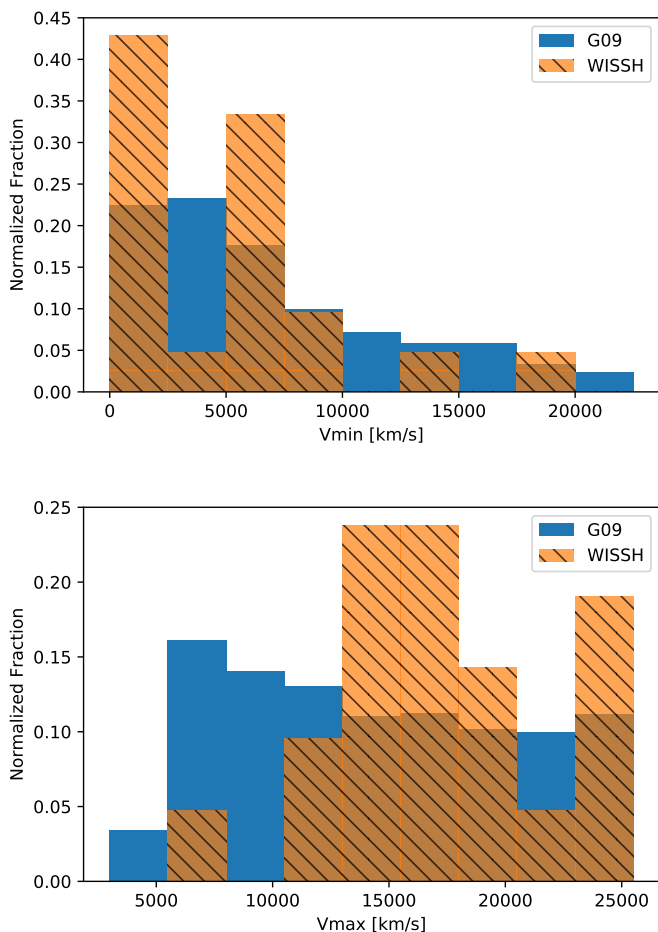


Fig. 3: Comparison between BI>0 BAL QSOs v_{min} and v_{max} in WISSH and G09 BAL QSOs catalogue.

conclusions on this trend and additional investigations based on larger samples of QSOs with $L_{bol} > 10^{47}$ erg/s are necessary.

3.4. Velocity distribution and potential for feedback of BAL QSOs

It is instructive to compare the distributions for the minimum and maximum velocities of the C iv BAL troughs (v_{min} and v_{max} , respectively), for all the BI>0 objects from both samples. We define as v_{min} and v_{max} the velocities estimated from the minimum and maximum wavelengths of the BAL troughs in the region between C iv and Si iv (values are given in Tab. 1). Normalized distributions for the two samples are plotted in Fig. 3. The v_{max} distribution seems clearly different between the two samples with the WISSH QSOs exhibiting a higher fraction at high velocities. A KS test gives a $p < 0.015$ for the v_{max} distribution from WISSH to be drawn from the same parent distribution as G09. This suggests that on average hyperluminous QSOs host the more extreme manifestations of the BAL phenomenon. On the other hand for the v_{min} distributions the test suggests no significant difference between the two samples ($p > 0.15$).

It is tempting to associate v_{max} to the terminal velocity reached at larger distances (Ganguly et al. 2007). This may imply a more efficient acceleration mechanism, for the most luminous QSOs, which pushes most of the winds up to $\gtrsim 15,000$ km s⁻¹, i.e. at the edge between the C iv and the Si iv emission lines used for

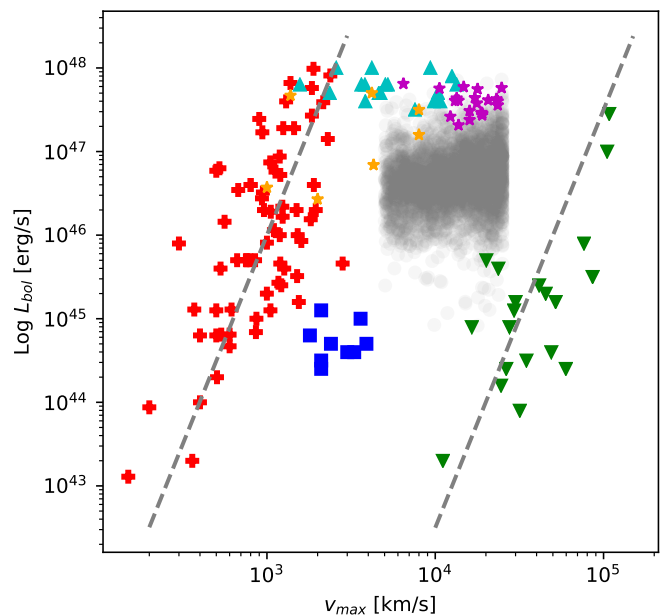


Fig. 4: Bolometric luminosities versus maximum wind velocity for the objects in Fiore et al. (2017) (red crosses: molecular and ionized winds; blue squares: warm absorbers; green downwards triangles: UFOs; orange stars: BALs), for WISSH BI>0 BAL QSOs (purple stars for the 21 C iv BALs), and for C iv winds from Vietri et al. (2018) (cyan upwards triangles). The region occupied by the G09 objects with BI>0 is in faded gray (note that the artificial v_{max} boundaries are a consequence of the BI selection).

the BI classification. As discussed above, the two UBOs show absorption even further blue-ward of the Si iv line: this further hints to a larger velocity distribution for the WISSH QSOs with even larger v_{max} values. These results show how QSOs with extreme luminosities such as the WISSH ones are able to accelerate BAL winds to larger velocities compared to AGN in lower luminosity regimes. Indeed, G09 found a highly significant correlation between $L_{\lambda 2500}$ and v_{max} , pointing towards a mainly radiative acceleration for the BAL winds, as suggested by previous authors (Murray & Chiang 1995; Laor & Brandt 2002).

In Fig. 4 we report L_{bol} as a function of v_{max} for a compilation of AGN-driven winds/outflows measured in different gas phases (molecular, ionized, warm absorbers, and UFOs). Data for molecular and ionized winds (red crosses), warm absorbers (blue squares), and UFOs (green downward triangles), have been collected by Fiore et al. (2017) with the specific aim of reporting properties of outflows with available estimates or limits on the physical distance of the high velocity gas from the central engine. Fig. 4 also includes the WISSH BI>0 BAL QSOs together with the incomplete but representative list of BAL QSOs provided by Fiore et al. (2017). Notice that the reported L_{bol} for the WISSH BAL QSOs are estimated through spectral energy distribution (SED) fitting (Duras et al. in prep.), while a good part of the sources reported in Fiore et al. (2017) have L_{bol} estimated also through bolometric correction factors. Fiore et al. (2017) found a log-linear relation between L_{bol} and v_{max} for both kpc-scale molecular/ionized and nuclear sub-pc relativistic winds with a similar slope of ~ 5 . The dependence is clearly visible in the plot in which more luminous sources tend to exhibit faster and nuclear/kpc-scale winds. In the plot we also report

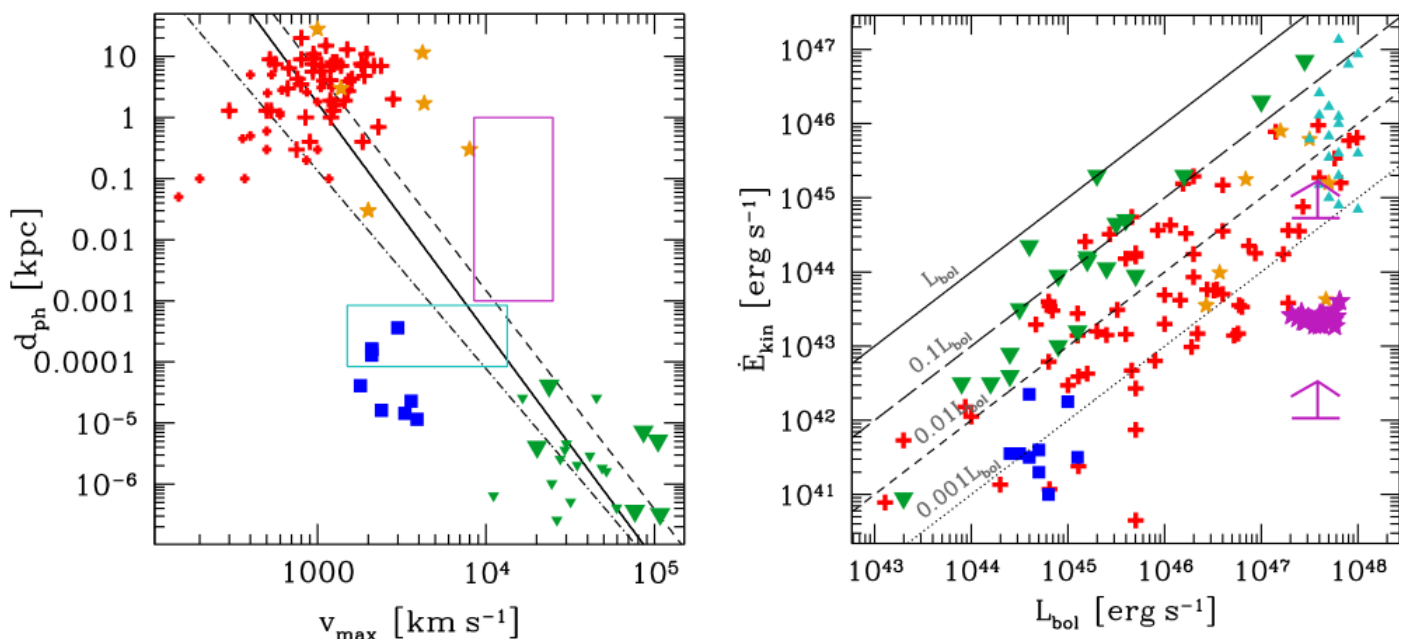


Fig. 5: Left panel: physical distance (d_{ph}) of the high velocity outflow component as a function of v_{max} for the same sources reported in Fig. 4 and belonging to the Fiore et al. (2017) sample. Large and small symbols for molecular/ionized kpc-scale outflows (red crosses) and UFOs (green triangles) represent sources with bolometric output higher and lower than $\log(L_{bol}/\text{erg s}^{-1}) = 45.5$. Solid, dot-dashed and dashed lines report a linear relations connecting the average points of kpc-scale outflows and UFOs for all sources, and sources fainter and brighter than $\log(L_{bol}/\text{erg s}^{-1}) = 45.5$, respectively. The position occupied by WISSH BALs and C IV broad emission line winds is reported by magenta and cyan rectangular regions, respectively (see text for details). Right panel: kinetic power as a function of bolometric luminosity for the sources reported in Fig. 4. The two lower limits represent our uncertainty on the BAL column density (see text for details).

the 21 C IV WISSH BAL QSOs with $BI > 0$ as purple stars. For comparison the position occupied by G09 $BI > 0$ BALs is also reported as faded grey region. Furthermore, we include broad C IV line nuclear winds detected as highly blueshifted emission lines (Vietri et al. 2018). We mention that the log-linear relations found by Fiore et al. (2017) normalized to the average v_{max} of the WISSH BALs nicely cover the region occupied by the G09 BALs, hinting to a possible similar relation for this wind phase despite the large spread of values in the G09 BALs.

In Fig. 5, left panel, we report the outflow physical distance (d_{ph}) measured for the high velocity gas as a function of v_{max} for kpc-scale outflows, WAs, BALs and UFOs, as reported in Fiore et al. (2017). We also include the locus occupied by BALs (purple rectangle) and C IV broad-emission-line nuclear winds (cyan rectangle) reported for the WISSH quasars. As these winds do not have an actual estimate of the distance, we adopted typical distances reported in literature studies. For WISSH BALs we adopt a range of 1 pc to 1 kpc (see e.g. Arav et al. 2018; Moravec et al. 2017; Leighly et al. 2018). For C IV broad-emission-line winds we adopt a range of $\sim 100 - 1000$ light-days typically found for luminous QSOs (e.g. $L_{bol} \approx 10^{47-48}$ erg/s) by reverberation mapping studies (e.g. Kaspi et al. 2007; Saturni et al. 2016). Notice that overall d_{ph} and v_{max} seem to anticorrelate with nuclear winds exhibiting faster winds than galaxy-scale outflows. We report in figure a linear relation joining the average points for kpc-scale outflow (red crosses) and UFOs (green triangles). There is an indication that this relation seems to be dependent on luminosity. Indeed dot-dashed and dashed lines report the relation for sources fainter and brighter than $\log(L_{bol}/\text{erg s}^{-1}) = 45.5$. Notice that given (i) the lack of uncertainties in the data included in the fit and (ii) the incompleteness of the sample used, this relation must not be considered as

universal but just as an broad-brush indication of the inverse relation. We find relations with slopes -3.6 and -3.2 and y-intercept 11.5 and 8.9 for bright and faint sources, respectively.

We use this relation between v_{max} and d_{ph} in order to estimate the maximum kinetic power \dot{E}_{kin} associated to BAL outflows in WISSH QSOs. We may infer \dot{E}_{kin} by dividing the kinetic energy $E_{kin} = 0.5Mv^2$ by a characteristic flow time given by d_{ph}/v_{max} . The kinetic energy is estimated as in Hamann et al. (2019). Their calculation assumes a spherical shell expanding at a certain velocity (v) with a given covering factor (Q) and thickness small compared to its radial distance (R). Under these assumptions E_{kin} is expressed by the following formula:

$$E_{kin}^{max} \approx 1.7 \times 10^{54} \left(\frac{Q}{0.28} \right) \left(\frac{N_H}{5 \times 10^{22} \text{ cm}^{-2}} \right) \left(\frac{R}{1 \text{ pc}} \right)^2 \times \left(\frac{v}{8000 \text{ km s}^{-1}} \right)^2 \text{ erg.} \quad (3)$$

For our calculation we assume $v = v_{max}$, $R = d_{ph}$ and $Q=0.28$ which is the average value derived from the literature (Trump et al. 2006; Knigge et al. 2008; Gibson et al. 2009; Allen et al. 2011). Since we do not have information on the column densities, and given that their estimate is beyond the aim of this work, we adopt a value of $N_H = 2.2 \times 10^{21} \text{ cm}^{-2}$. The latter is the logarithmic mean value between of $N_H = 10^{20} \text{ cm}^{-2}$ and $N_H = 5 \times 10^{22} \text{ cm}^{-2}$ which are minimum column densities derived from doubly and triply ionized species (Arav et al. 2018) and P v troughs (Hamann et al. 2019), respectively. In Fig. 5, right panel, we report the \dot{E}_{kin} estimated for the WISSH BALs as a function of L_{bol} compared to the same values reported for other winds/outflows by Fiore et al. (2017) and Vietri et al. (2018). We report as lower limits, the values of \dot{E}_{kin} estimated at the minimum N_H reported for low column density (Arav et al. 2018)

and high column density (i.e. from P v troughs, Arav et al. 2018) winds. Notice that the densest winds can reach values of kinetic power which are of the order of $\gtrsim 0.1\%$ of the bolometric luminosity. Even higher values are expected if the luminosity dependence of the $d_{ph} - v_{max}$ relation holds at highest luminosities. Notice that we are making the assumption that the most of the outflowing mass is carried at v_{max} . If instead we adopt v_{min} as representative phase for carrying the majority of the kinetic power of the wind, then by adopting the lowest value of $d_{ph} = 1$ pc, we obtain a lower limit on \dot{E}_{kin} which is one order of magnitude lower. Bearing in mind the crude assumptions in this estimate, this is an indication that some of these winds are in principle able to transport a kinetic power sufficient for generating a significant feedback contribution on the host (Di Matteo et al. 2005; Hopkins & Elvis 2010).

3.5. Multiple AGN winds in WISSH quasars

In Bischetti et al. (2017) and Vietri et al. (2018) we revealed the presence of kpc- and BLR-scale winds in WISSH objects by detecting a broad/blue-shifted $[OIII]$ or C IV emission lines in the rest-frame, optical, and UV spectra of a randomly-selected sub-sample of 18 WISSH QSOs. Among them, seven objects (namely 1157+27, 1326-00, 1421+46, 1422+44, 1538+08, 1549+12 and 2123-00) exhibit absorption features in their SDSS spectra (see Table 1). Specifically, they all show an $AI_{1000} > 0$ km/s, and for four sources we derive a positive BI. Vietri et al. (2018) reported the existence of two sub-populations of WISSH QSOs based on their emission line properties. The first one (consisting of six sources, dubbed $[OIII]$) is characterized by a broad $[OIII]$ emission line, a Rest-frame Equivalent Width (REW) of the C IV emission $REW_{CIV} \approx 20-40 \text{ \AA}$ and a profile of the C IV emission line blueshifted of $< 2,000$ km/s. The second one (dubbed *Weak [OIII]* sources, and representing two-thirds of the LBT/LUCI WISSH sample) exhibits weak/absent $[OIII]$ emission, and a highly-blue-shifted (2,000 – 8,000 km/s) C IV emission line with $REW < 20 \text{ \AA}$.

Vietri et al. (2018) interpreted the dichotomy observed in WISSH QSOs in terms of a combination of huge ionizing flux (leading to overionization of the NLR gas and, hence, a decrease of the $[OIII]$ emission, e.g. Shen & Ho 2014) and inclination. In particular, for *Weak [OIII]* QSOs the accretion disk is seen face-on, while $[OIII]$ ones should be viewed at larger inclination angles, i.e. $\theta \sim 25-70$ degrees. Interestingly, intermediate inclinations ($\sim 25-40$ degrees) for BAL QSOs have been also suggested by Elvis (2000).

Among the seven QSOs with $AI > 0$ km/s, three belong to the $[OIII]$ subclass, while four are *Weak [OIII]* objects. Two out of three $[OIII]$ QSOs are classified as BAL according to BI, while the remaining one (1326-00) has $AI_{1000} \gtrsim 2,000$ km/s. This is quite interesting and suggests that the simultaneous presence of BAL and kpc-scale outflows may be common at the highest AGN luminosities. On the contrary, only one *Weak [OIII]* QSO (1157+27) shows a $BI > 0$ km/s, and all the remaining ones only have modest ($\lesssim 300$ km/s) AI. Future follow-up studies of the $[OIII]$ emission in a larger sample of luminous BAL QSOs will be crucial to support this orientation scenario for the simultaneous detection of NLR and BAL outflows.

4. Radio properties of WISSH BAL QSOs

We cross-correlated the BAL QSOs list from WISSH with the FIRST catalogue (Becker et al. 1995), using a 5" matching radius

centered on the optical coordinates, in order to determine the fraction of WISSH BAL QSOs with a radio counterpart. Eight over 38 ($\sim 21\%$) have a counterpart in FIRST, namely 0747+27, 1025+24, 1130+07, 1204+33, 1237+06, 1422+44, 1513+08, and 1549+12. As a whole, 20 over 86 objects ($\sim 23\%$) in WISSH have a radio counterpart.

Shankar et al. (2008) studied the dependence of the BAL QSOs fraction among the radio population as a function of specific luminosity at 1.4 GHz ($L_{1.4GHz}$, from FIRST). They found that it can drop from $\sim 20\%$ to $\sim 8\%$ when moving from an $L_{1.4GHz} \sim 10^{32}$ to $\sim 10^{36}$ erg/s/Hz for BI-selected BAL QSOs, while from $\sim 45\%$ to $\sim 20\%$ for the AI-selected ones. No entirely satisfactory physical model was found for such a behavior, both the evolutionary and geometrical one not reflecting the complex phenomenology of these objects. The $L_{1.4GHz}$ range for the WISSH sample is $8 \times 10^{31} - 2 \times 10^{35}$ erg/s/Hz (see Fig. 6), similar to the one explored by those authors. This was calculated from the FIRST flux density as in equation 1 of Shankar et al. (2008), but assuming a spectral index $\alpha=0$ since both inverted and steep spectral indices have been found in samples of radio-loud BAL QSOs (Montenegro-Montes et al. 2008; DiPompeo et al. 2011; Bruni et al. 2012) - although, as discussed in Shankar et al. (2008), the estimate has only a weak dependence on α . Despite the poor statistic - only 8 among the 20 WISSH object with a radio counterpart are BAL QSOs - the fraction we find at luminosities $L_{1.4GHz} < 10^{33}$ erg/s/Hz is $\sim 47\%$ when considering objects with $AI > 0$, and $\sim 20\%$ when considering the ones with $BI > 0$, in agreement with the trend found by those authors.

From a morphological point of view, images from FIRST show a compact morphology for all sources, corresponding to an upper limit for linear sizes of ~ 40 kpc at the mean redshift of the BAL QSOs subsample in WISSH ($z=3.2$). This is in agreement with linear sizes from previous studies at arcsec angular resolution (Bruni et al. 2012), resulting in a compact radio morphology, < 40 kpc, for more than 90% of objects at a similar redshift range.

The radio properties presented here do not suggest a behavior different from previous samples, despite the extreme luminosity regime in WISSH. The coupling between the BAL-producing winds and the jet seems to have trends similar to the ones presented in previous works from the literature, meaning that the higher probability for WISSH objects to launch winds does not imply different jet formation rates or strength.

5. Conclusions

We have analysed the properties of the BAL QSOs fraction in the WISSH sample, composed by hyper-luminous type-1 AGN, and compared to those of BAL QSOs from the literature. Results can be summarized as follows:

- Adopting the standard BAL indices, we found in WISSH 38 objects with an $AI > 0$ ($44 \pm 7\%$), 32 with $AI_{1000} > 0$ ($37 \pm 6\%$), and 21 with $BI > 0$ ($24 \pm 5\%$).
- The fraction of objects with a C IV $BI > 0$ (24%) is almost two times higher than what found in G09. Also, the BI distributions for the two samples are distinct, with typically higher values for the WISSH sample. The LoBAL fraction among BAL QSOs in WISSH is $\sim 26\%$, which is also larger than what found at similar luminosities in previous works. The higher L_{bol} of the WISSH objects likely favours the acceleration of BAL outflows (in both the high- and low-ionization

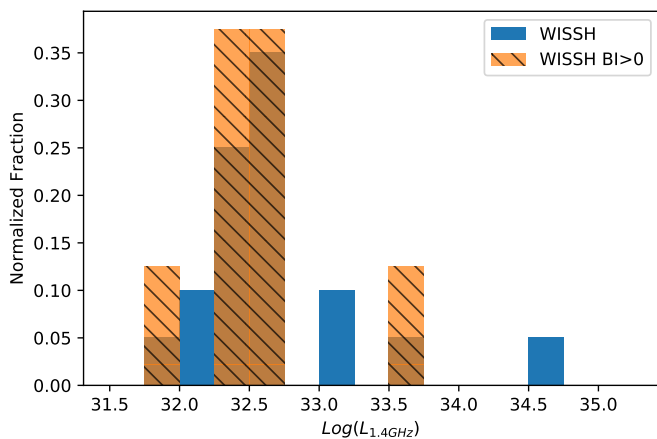


Fig. 6: Normalized distributions of $L_{1.4\text{GHz}}$ for all WISSH objects with FIRST radio counterpart (blue) and for BAL QSOs in WISSH with FIRST radio counterpart (orange).

gas components), indicating that they are likely radiatively driven.

- The maximum velocities of the C iv BAL outflows in WISSH have a different distribution from those in G09, with WISSH QSOs exhibiting larger values. This lends further support to the theoretical predictions suggesting that, via radiative pressure, hyper-luminous QSOs are able to launch the most extreme winds (Giustini & Proga 2019).
- We find two QSOs exhibiting BAL features with velocities of $\sim 0.15c$, by assuming that absorption blue-wards of the Si iv emission line is associated with C iv. Although the statistics is very limited (i.e. 2 with respect to the 21 objects showing a BI > 0), this seems to lend further support to a scenario where hyper-luminous QSOs are able to accelerate the most powerful outflows (e.g. Laor & Brandt 2002; Fiore et al. 2017)
- We estimate the possible range of kinetic power associated to BAL outflows in WISSH which can reach values above 0.1% of L_{bol} . This indicates that, especially for the highest column density and fastest winds, BAL outflows in hyperluminous QSOs are potentially able to provide an efficient feedback onto the host galaxy interstellar medium.
- About 20% of BI-selected BAL QSOs from WISSH shows a radio counterpart in FIRST (1.4 GHz), this fraction being compatible with the one found in G09 (23%). It also confirms that the WISSH sample shows the same anti-correlation between $L_{1.4\text{GHz}}$ and BAL QSOs abundance found by Shankar et al. (2008), not indicating any particular dependence of the BAL QSOs radio properties on the L_{bol} .

Future works based on much larger samples of hyper-luminous QSOs are needed to shed more light on the crucial role of L_{bol} in increasing the fraction and the power of BAL outflows in the QSO population.

Acknowledgements. We thank the anonymous referee for the constructive comments and suggestions. GB acknowledges financial support under the INTEGRAL ASI-INAF agreement 2013-025-R.1. EP acknowledges financial support from the Italian Space Agency (ASI) under the contracts ASI-INAF I/037/12/0 and ASI-INAF n.2017-14-H.0. LZ acknowledges financial support under ASI-INAF contract I/037/12/0. FT acknowledges support by the Programma per Giovani Ricercatori - anno 2014 Rita Levi Montalcini. This research project was supported by the DFG Cluster of Excellence ‘Origin and Structure of the Universe’ (www.universe-cluster.de). Funding for the Sloan Digital Sky

Survey IV has been provided by the Alfred P. Sloan Foundation, the U.S. Department of Energy Office of Science, and the Participating Institutions. SDSS-IV acknowledges support and resources from the Center for High-Performance Computing at the University of Utah. The SDSS web site is www.sdss.org. SDSS-IV is managed by the Astrophysical Research Consortium for the Participating Institutions of the SDSS Collaboration including the Brazilian Participation Group, the Carnegie Institution for Science, Carnegie Mellon University, the Chilean Participation Group, the French Participation Group, Harvard-Smithsonian Center for Astrophysics, Instituto de Astrofísica de Canarias, The Johns Hopkins University, Kavli Institute for the Physics and Mathematics of the Universe (IPMU) / University of Tokyo, the Korean Participation Group, Lawrence Berkeley National Laboratory, Leibniz Institut für Astrophysik Potsdam (AIP), Max-Planck-Institut für Astronomie (MPIA Heidelberg), Max-Planck-Institut für Astrophysik (MPA Garching), Max-Planck-Institut für Extraterrestrische Physik (MPE), National Astronomical Observatories of China, New Mexico State University, New York University, University of Notre Dame, Observatório Nacional / MCTI, The Ohio State University, Pennsylvania State University, Shanghai Astronomical Observatory, United Kingdom Participation Group, Universidad Nacional Autónoma de México, University of Arizona, University of Colorado Boulder, University of Oxford, University of Portsmouth, University of Utah, University of Virginia, University of Washington, University of Wisconsin, Vanderbilt University, and Yale University.

References

- Alam, S., Albareti, F. D., Allende Prieto, C., et al. 2015, *The Astrophysical Journal Supplement Series*, 219, 12
- Allen, J. T., Hewett, P. C., Maddox, N., Richards, G. T., & Belokurov, V. 2011, *MNRAS*, 410, 860
- Arav, N., Borguet, B., Chamberlain, C., Edmonds, D., & Danforth, C. 2013, *MNRAS*, 436, 3286
- Arav, N., Liu, G., Xu, X., et al. 2018, *ApJ*, 857, 60
- Becker, R. H., White, R. L., Gregg, M. D., et al. 2000, *ApJ*, 538, 72
- Becker, R. H., White, R. L., & Helfand, D. J. 1995, *ApJ*, 450, 559
- Bischetti, M., Piconcelli, E., Feruglio, C., et al. 2019, arXiv e-prints, arXiv:1903.10528
- Bischetti, M., Piconcelli, E., Vietri, G., et al. 2017, *A&A*, 598, A122
- Bruni, G., Dallacasa, D., Mack, K. H., et al. 2013, *A&A*, 554, A94
- Bruni, G., Mack, K. H., Salerno, E., et al. 2012, *A&A*, 542, A13
- Cicone, C., Maiolino, R., Sturm, E., et al. 2014, *A&A*, 562, A21
- Costa, T., Sijacki, D., & Haehnelt, M. G. 2014, *MNRAS*, 444, 2355
- Dai, X., Shankar, F., & Sivakoff, G. R. 2008, *ApJ*, 672, 108
- Di Matteo, T., Springel, V., & Hernquist, L. 2005, *Nature*, 433, 604
- DiPompeo, M. A., Brotherton, M. S., De Breuck, C., & Laurent-Muehleisen, S. 2011, *ApJ*, 743, 71
- Dunn, J. P., Arav, N., Aoki, K., et al. 2012, *ApJ*, 750, 143
- Duras, F., Bongiorno, A., Piconcelli, E., et al. 2017, *A&A*, 604, A67
- Elvis, M. 2000, *ApJ*, 545, 63
- Fabian, A. C. 2012, *Annual Review of Astronomy and Astrophysics*, 50, 455
- Feruglio, C., Fiore, F., Carniani, S., et al. 2015, *A&A*, 583, A99
- Fiore, F., Feruglio, C., Shankar, F., et al. 2017, *A&A*, 601, A143
- Ganguly, R., Brotherton, M. S., Cales, S., et al. 2007, *ApJ*, 665, 990
- Gehrels, N. 1986, *ApJ*, 303, 336
- Gibson, R. R., Jiang, L., Brandt, W. N., et al. 2009, *ApJ*, 692, 758
- Giustini, M. & Proga, D. 2019, arXiv e-prints [arXiv:1904.07341]
- Gregg, M. D., Becker, R. H., & de Vries, W. 2006, *ApJ*, 641, 210
- Haiman, Z. & Bryan, G. L. 2006, *ApJ*, 650, 7
- Hall, P. B., Anderson, S. F., Strauss, M. A., et al. 2002, *The Astrophysical Journal Supplement Series*, 141, 267
- Hamann, F., Chartas, G., McGraw, S., et al. 2013, *MNRAS*, 435, 133
- Hamann, F., Chartas, G., Reeves, J., & Nardini, E. 2018, *MNRAS*, 476, 943
- Hamann, F., Herbst, H., Paris, I., & Capellupo, D. 2019, *MNRAS*, 483, 1808
- Hemler, Z. S., Grier, C. J., Brandt, W. N., et al. 2019, *ApJ*, 872, 21
- Hewett, P. C. & Foltz, C. B. 2003, *AJ*, 125, 1784
- Hewett, P. C., Foltz, C. B., & Chaffee, F. H. 1995, *AJ*, 109, 1498
- Hopkins, P. F. & Elvis, M. 2010, *MNRAS*, 401, 7
- Kaspi, S., Brandt, W. N., Maoz, D., et al. 2007, *ApJ*, 659, 997
- Knigge, C., Scaringi, S., Goad, M. R., & Cottis, C. E. 2008, *MNRAS*, 386, 1426
- Kraemer, S. B., Tombesi, F., & Bottorff, M. C. 2018, *ApJ*, 852, 35
- Laor, A. & Brandt, W. N. 2002, *ApJ*, 569, 641
- Leighly, K. M., Terndrup, D. M., Gallagher, S. C., Richards, G. T., & Dietrich, M. 2018, *ApJ*, 866, 7
- Li, Y., Hernquist, L., Robertson, B., et al. 2007, *ApJ*, 665, 187
- Martocchia, S., Bastian, N., Usher, C., et al. 2017, *MNRAS*, 468, 3150
- Martzeu, G. A., Reeves, J. N., Braito, V., et al. 2017, *MNRAS*, 472, L15
- Menci, N., Fiore, F., Puccetti, S., & Cavaliere, A. 2008, *ApJ*, 686, 219
- Montenegro-Montes, F. M., Mack, K. H., Vigotti, M., et al. 2008, *MNRAS*, 388, 1853

- Moravec, E. A., Hamann, F., Capellupo, D. M., et al. 2017, MNRAS, 468, 4539
- Murray, N. & Chiang, J. 1995, ApJ, 454, L105
- Pâris, I., Petitjean, P., Aubourg, É., et al. 2018, A&A, 613, A51
- Pâris, I., Petitjean, P., Aubourg, É., et al. 2014, A&A, 563, A54
- Pâris, I., Petitjean, P., Ross, N. P., et al. 2017, A&A, 597, A79
- Planck Collaboration, Aghanim, N., Akrami, Y., et al. 2018, ArXiv e-prints, arXiv:1807.06209
- Proga, D. 2000, ApJ, 538, 684
- Reichard, T. A., Richards, G. T., Schneider, D. P., et al. 2003, AJ, 125, 1711
- Risaliti, G. & Elvis, M. 2010, A&A, 516, A89
- Rodríguez-Hidalgo, P., Hamann, F., & Hall, P. 2011, Monthly Notices of the Royal Astronomical Society, 411, 247
- Rogerson, J. A., Hall, P. B., Rodríguez Hidalgo, P., et al. 2016, MNRAS, 457, 405
- Saturni, F. G., Trevese, D., Vagnetti, F., Perna, M., & Dadina, M. 2016, A&A, 587, A43
- Shankar, F., Dai, X., & Sivakoff, G. R. 2008, ApJ, 687, 859
- Shen, Y. & Ho, L. C. 2014, Nature, 513, 210
- Shen, Y., Richards, G. T., Strauss, M. A., et al. 2011, The Astrophysical Journal Supplement Series, 194, 45
- Silk, J. & Rees, M. J. 1998, A&A, 331, L1
- Sprayberry, D. & Foltz, C. B. 1992, ApJ, 390, 39
- Tadhunter, C., Morganti, R., Rose, M., Oonk, J. B. R., & Oosterloo, T. 2014, Nature, 511, 440
- Tombesi, F., Cappi, M., Reeves, J. N., et al. 2013, MNRAS, 430, 1102
- Tombesi, F., Cappi, M., Reeves, J. N., et al. 2011, ApJ, 742, 44
- Tombesi, F., Cappi, M., Reeves, J. N., et al. 2010, A&A, 521, A57
- Tombesi, F., Meléndez, M., Veilleux, S., et al. 2015, Nature, 519, 436
- Trump, J. R., Hall, P. B., Reichard, T. A., et al. 2006, The Astrophysical Journal Supplement Series, 165, 1
- Vietri, G., Piconcelli, E., Bischetti, M., et al. 2018, A&A, 617, A81
- Weymann, R. J., Morris, S. L., Foltz, C. B., & Hewett, P. C. 1991, ApJ, 373, 23
- Wyithe, J. S. B. & Loeb, A. 2003, ApJ, 595, 614
- York, D. G., Adelman, J., Anderson, John E., J., et al. 2000, AJ, 120, 1579
- Zubovas, K. & King, A. 2012, ApJ, 745, L34

Appendix A: BAL QSOs spectra

We report here the SDSS DR12 spectra of the 38 BAL QSOs presented in this work. For each object, we show the spectrum, the combined continuum and emission lines fit performed in IRAF, the Si IV and C IV peaks position as calculated from redshift (dashed gray lines), and the residuals used for the BAL indices integrals calculation (from 0 to 25,000 km/s), where the absorption below 90% of the continuum is highlighted in orange. We also mark the v_{min} and v_{max} estimates for each object as dashed orange lines.

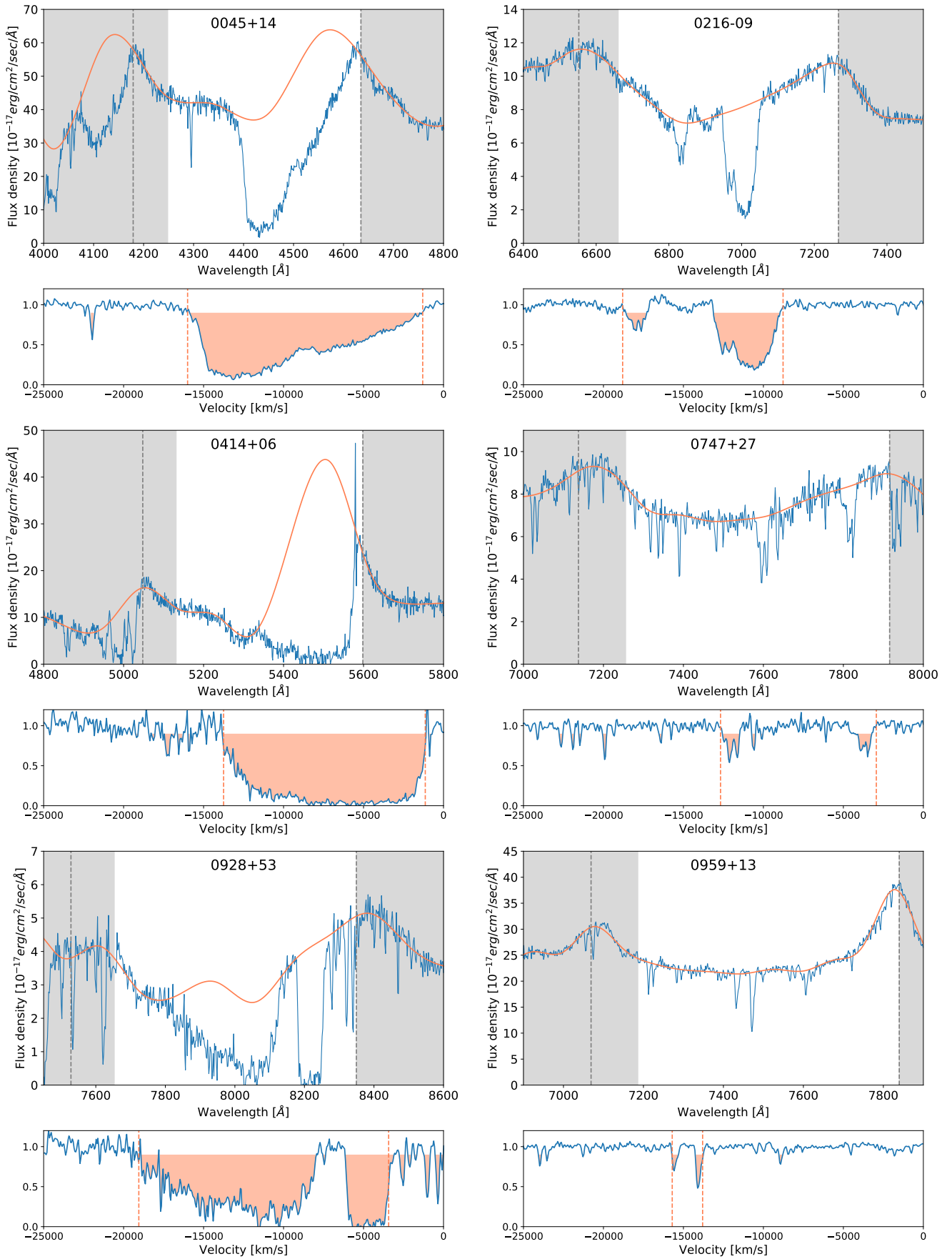


Fig. A.1: SDSS DR12 spectra of the 38 BAL QSOs presented here. Top panel: spectrum (blue line) and fit performed in IRAF (orange line); dashed lines indicate the position of the Si iv and C iv peaks as calculated from redshift, while the white area the wavelengths interval between 0 and $-25,000$ km/s. Bottom panel: residuals between the C iv peak and $-25,000$ km/s, with absorption below 90% of the continuum highlighted in orange; dashed lines indicate the minimum and maximum velocity estimated for the BAL outflow.

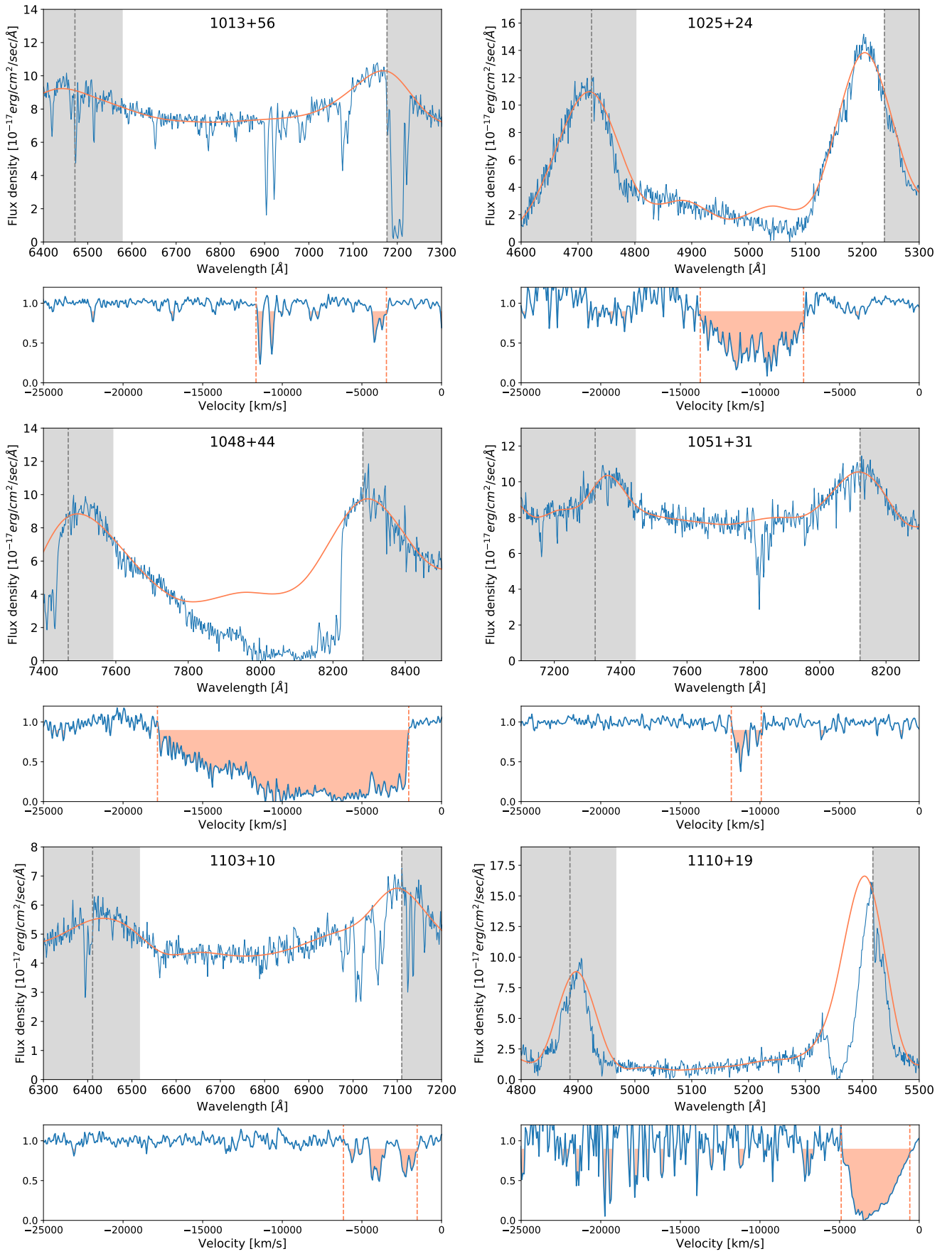


Fig. A.1: Continued

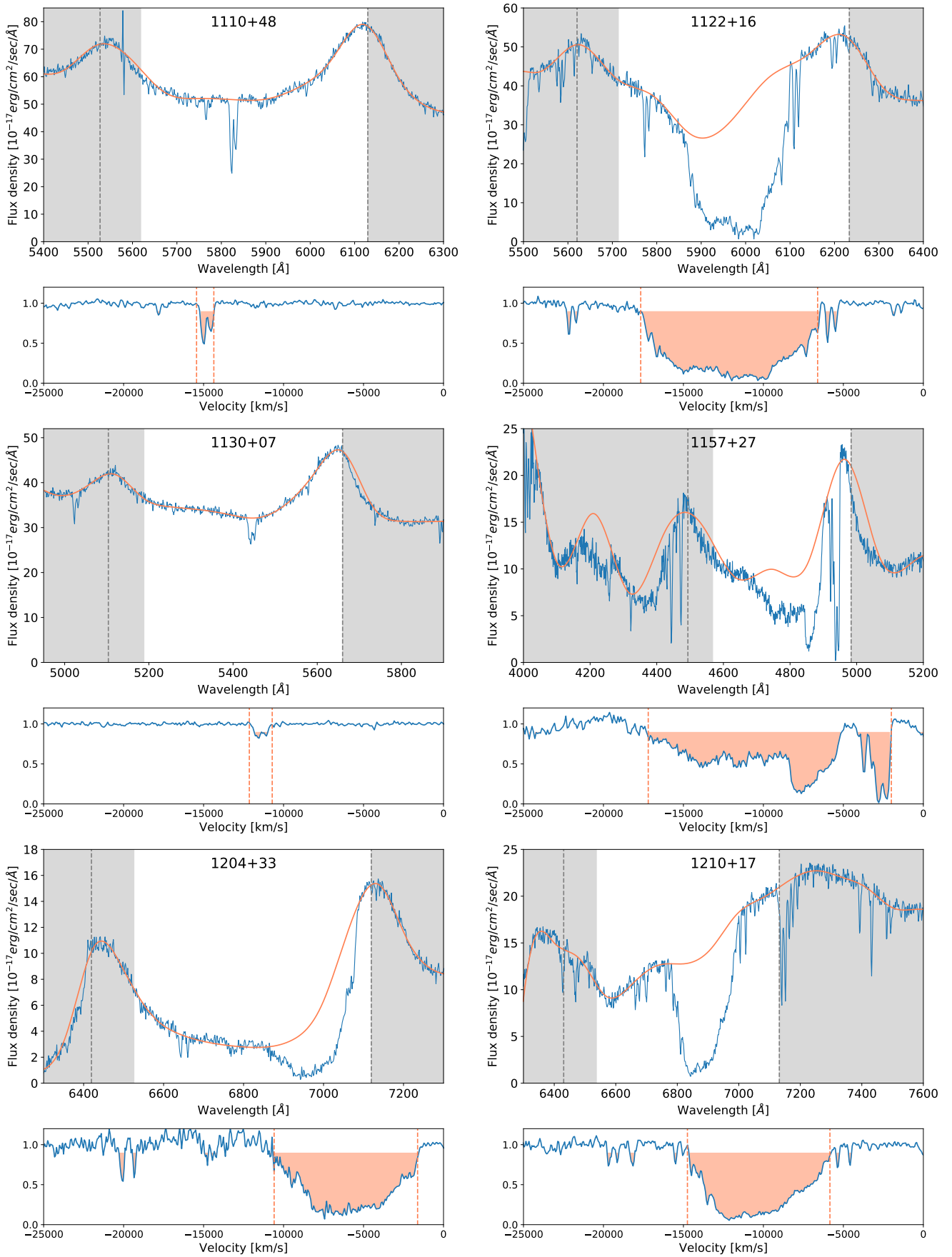


Fig. A.1: Continued

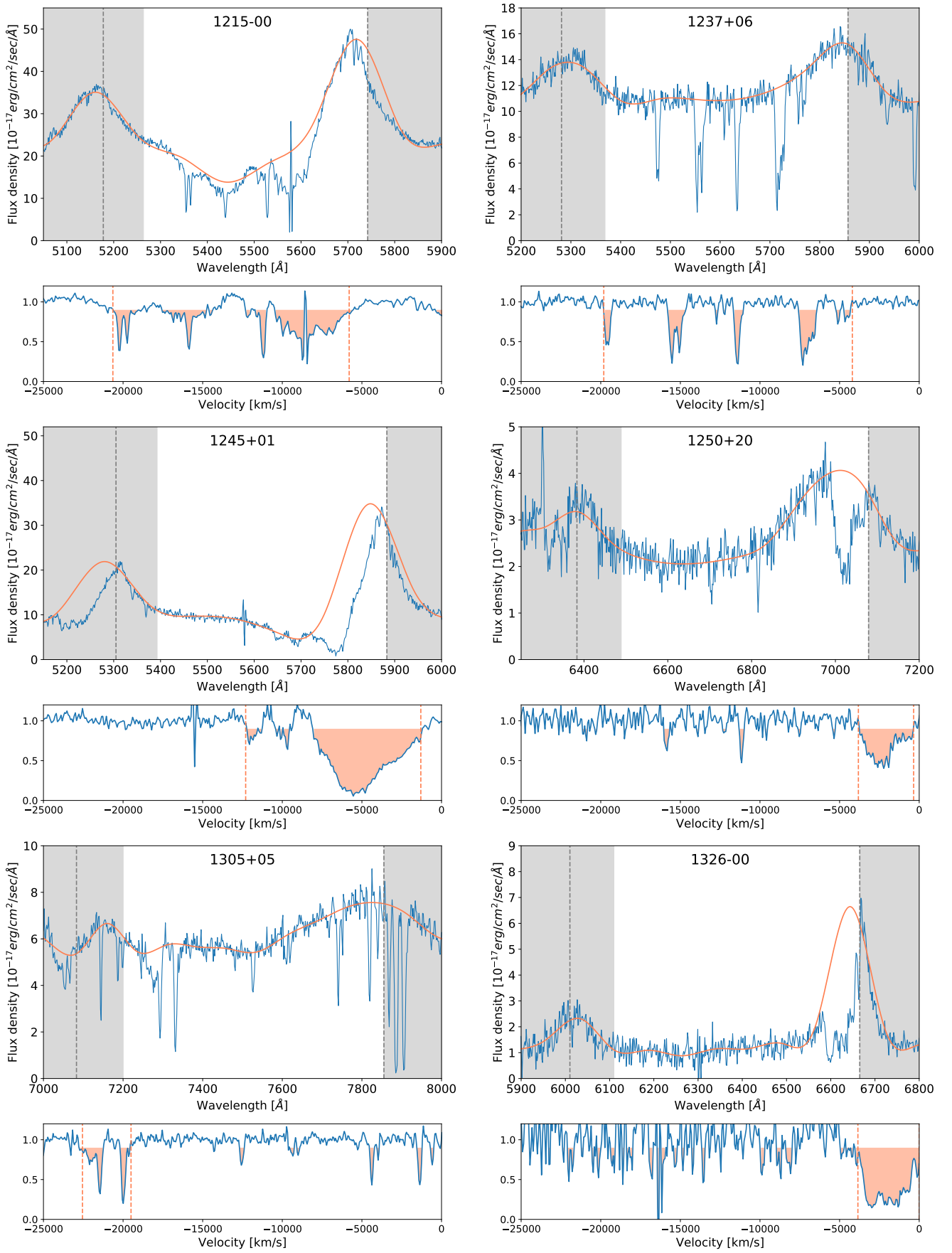


Fig. A.1: Continued

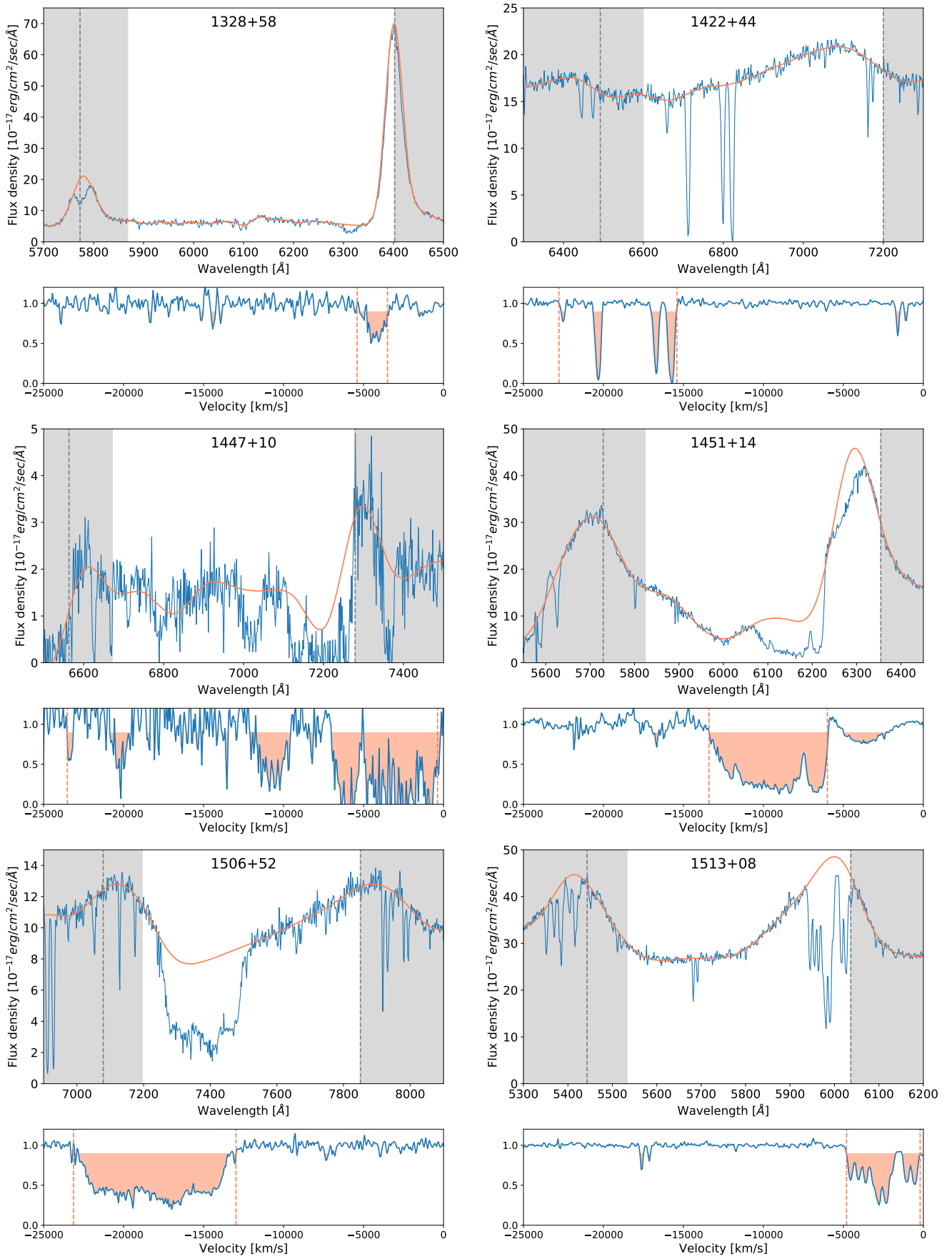


Fig. A.1: Continued

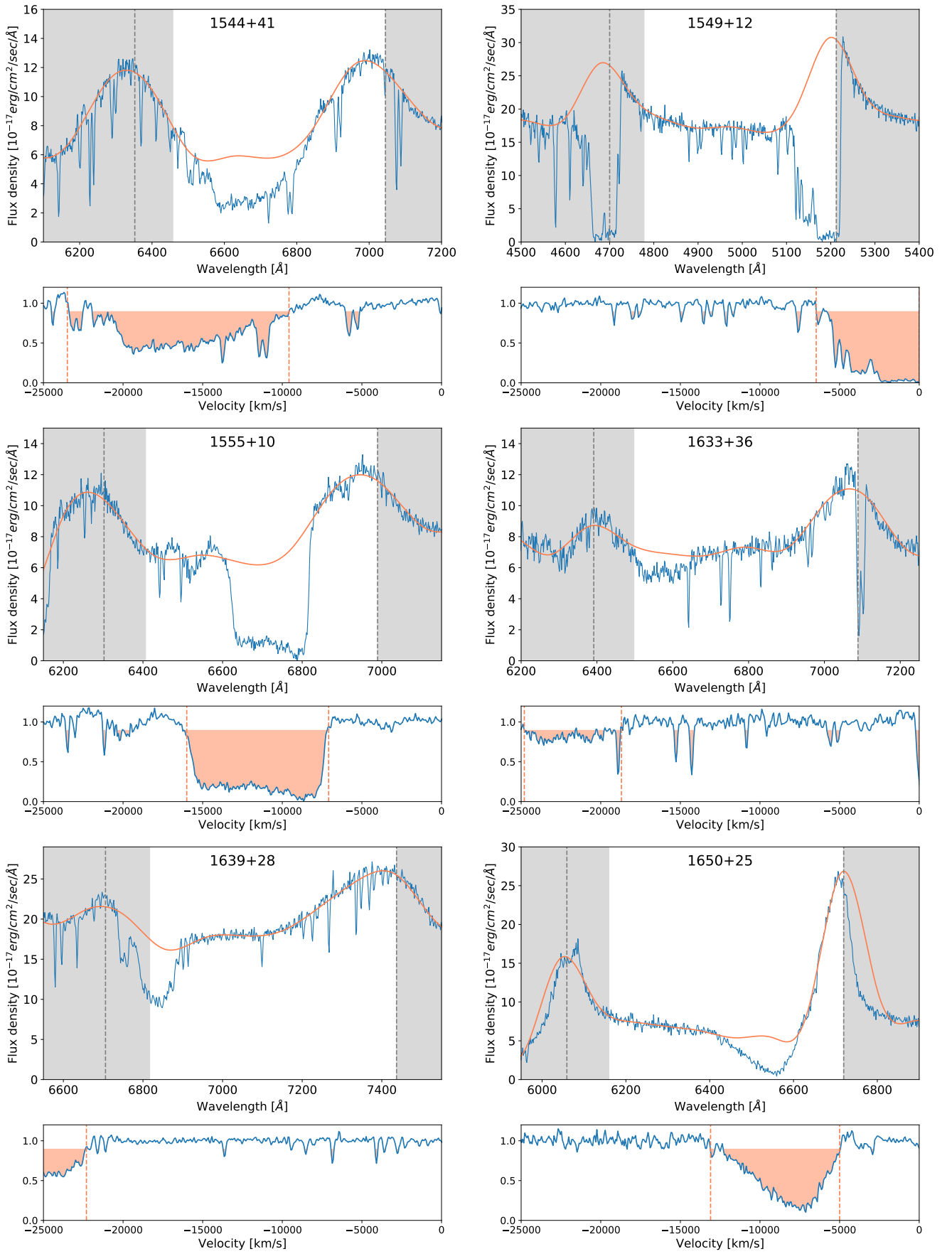


Fig. A.1: Continued

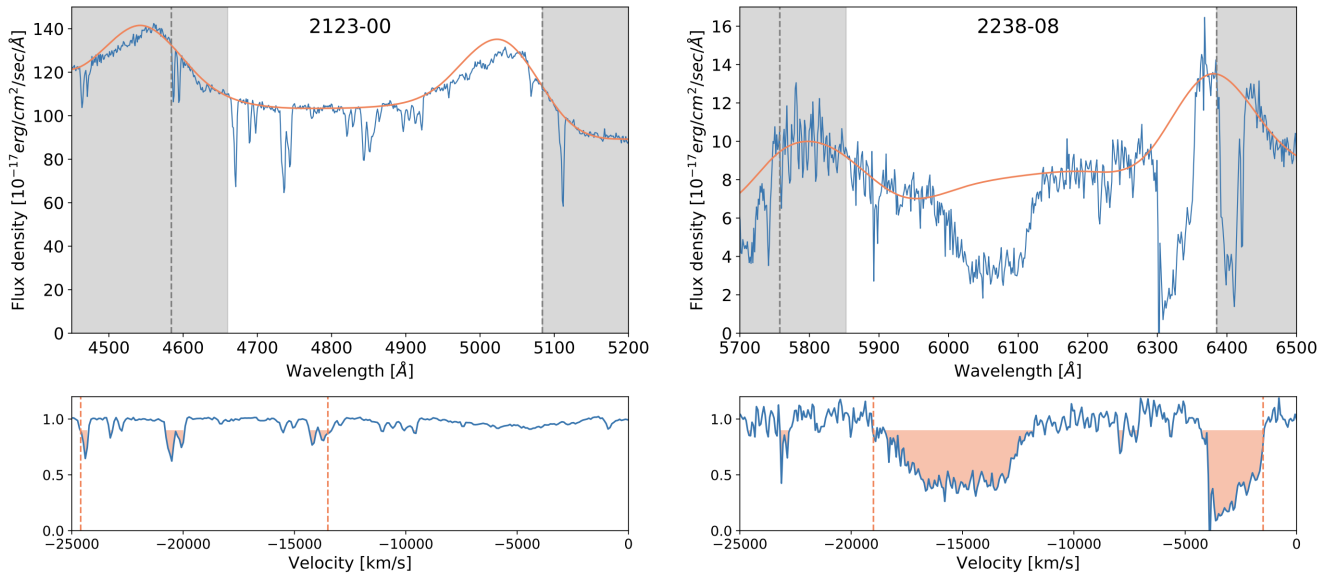


Fig. A.1: Continued